Accommodation at the interface of highly dissimilar semiconductor/oxide epitaxial systems

G. Saint-Girons,[1,*] J. Cheng,[1] P. Regreny,[1] L. Largeau,[2] G. Patriarche,[2] and G. Hollinger[1]
[1]*Ecole Centrale de Lyon, INL-UMR 5270/CNRS, Université de Lyon, 36 Avenue Guy de Collongue, 69134 Ecully Cedex, France*
[2]*LPN-UPR 20, CNRS, Route de Nozay, 91460 Ecully Cedex, France*

(Received 10 February 2009; revised manuscript received 11 September 2009; published 7 October 2009)

An equilibrium model describing accommodation at epitaxial interfaces of highly dissimilar material systems is presented. For large lattice mismatches and large interface energies, the material nucleates with its bulk lattice parameter, mismatch being accommodated by interface dislocations. No threading defects are formed, contrasting with standard plastic relaxation mechanisms. It is shown that good quality InP can be grown on $SrTiO_3$ (STO) despite the large mismatch. This opens perspectives for the monolithic integration of InP on STO/Si templates and for the widening of the application spectrum of heteroepitaxy.

DOI: 10.1103/PhysRevB.80.155308 PACS number(s): 68.35.−p, 68.55.A−, 81.10.−h

I. INTRODUCTION

Lattice mismatch is a major limitation of heteroepitaxy: in a widely shared vision of epitaxial process (designated as lattice matched epitaxy by Narayan *et al.*),[1] a mismatched layer takes the in-plane lattice parameter of the substrate at the beginning of the growth, thus undergoing an elastic deformation. Above a so-called critical thickness, a plastic relaxation process occurs during which threading dislocations are formed in the growing layer.[2] This leads to significant degradation of its structural and electronic properties, strongly limiting the applicative spectrum of epitaxial techniques. Overcoming this limitation is a key issue of the future development of microelectronic and optoelectronic systems. Integrating III-V semiconductors on silicon could lead to the association of micro and optoelectronic functionalities on the same silicon basewafer, to the fabrication of high mobility III-V channels on Si, and would allow fabricating III-V/Si templates that would advantageously replace the size-limited III-V substrates, thus leading to major breakthrough in the field of photovoltaics. Heterogeneous integration techniques, based on substrate bonding, have reached an advanced degree of maturity. However, these approaches are limited by their technological complexity, and do not allow full wafer treatments. Several approaches of monolithic integration have been investigated. Most of them rely on the use of thick plastically relaxed buffers,[3–5] of so-called compliant substrates which adapt their lattice parameter to the one of the layer to be grown,[6–8] or on substrate prepatterning techniques.[9] They remain limited by their technological complexity and by the resulting poor quality of the integrated layers, and are based on the idea that a mismatched material is inevitably strained on its substrate at the early stages of its growth.

Several studies have given some theoretical and/or experimental descriptions of so-called "highly dissimilar" epitaxial systems.[10–13] Recently, the possibility of growing good quality crystalline $SrTiO_3$ (STO) on Si substrates has been demonstrated.[14–16] On this basis, Motorola has published controversial results on the monolithic fabrication of GaAs MESFETs on silicon, without clarifying any growth or material issue.[17–19] More recently, we have given experimental evidence of the spontaneous compliance of InP/STO(001) and InP/Gd_2O_3(111) heterointerfaces.[20,21] In this paper, we propose an equilibrium model that clarifies the origin of the compliance of highly dissimilar epitaxial systems, and particularly of the semiconductor/oxide systems. Our approach accounts for the interface energy and for the existence of a critical nucleation volume. With the exception of the molecular dynamics calculations of the interface energy described in Ref. 22, most of the existing models[23–26] neglect these parameters despite their crucial influence on the growth, particularly for highly dissimilar material systems. On the basis of our model, we show how the growth of InP on STO can be controlled to obtain layers compatible with applicative requirements.

II. EQUILIBIRUM NUCLEATION MODEL FOR HIGHLY DISSIMILAR EPITAXIAL SYSTEMS

At the very early stages of epitaxy, on condition that the chemical potential difference between gas and solid phases is positive, condensation thermodynamics predict the existence of a critical nucleation volume V_c above which nuclei formed at the substrate surface are stable.[27] This critical volume is obtained by maximizing the nucleation free enthalpy ΔG as a function of volume (Eq. (1)):

$$\Delta G = V \times (E_V - \Delta\mu) + (\gamma_{AB} - \gamma_B) \times S_{AB} + \gamma_i \times S_i, \quad (1)$$

where E_V is the elastic energy stored in the deposit per unit of volume, γ_{AB}, γ_B, and γ_i are the interface, substrate, and deposit surface energies, respectively, S_{AB} is the contact surface between deposit A and substrate B, S_i is the free surface of the deposit, and $\Delta\mu$ is the chemical potential difference per unit of volume of the deposit between the gas phase and the solid phase. The growth can either be three-dimension (3D) or two-dimension (2D). For the sake of generality, we consider here 3D islands as spherical caps, defined by their volume V and their inverse aspect ratio $q=d/h$, where d and h are defined in Fig. 1. 2D islands are described as cylindrical platelets with a diameter d and a height h equal to one monolayer. Maximizing ΔG leads to following expressions of the 2D and 3D critical nucleation volumes:

$$V_C^{3D} = \left(\frac{2}{3} \cdot L \cdot \frac{\pi}{4}\left(\frac{2}{\pi}\right)^{2/3} \cdot \frac{4 + q^2(1+\alpha_B)}{(1-\alpha_c)\cdot(1/3 + q^2/4)^{2/3}}\right)^3 \quad (2)$$

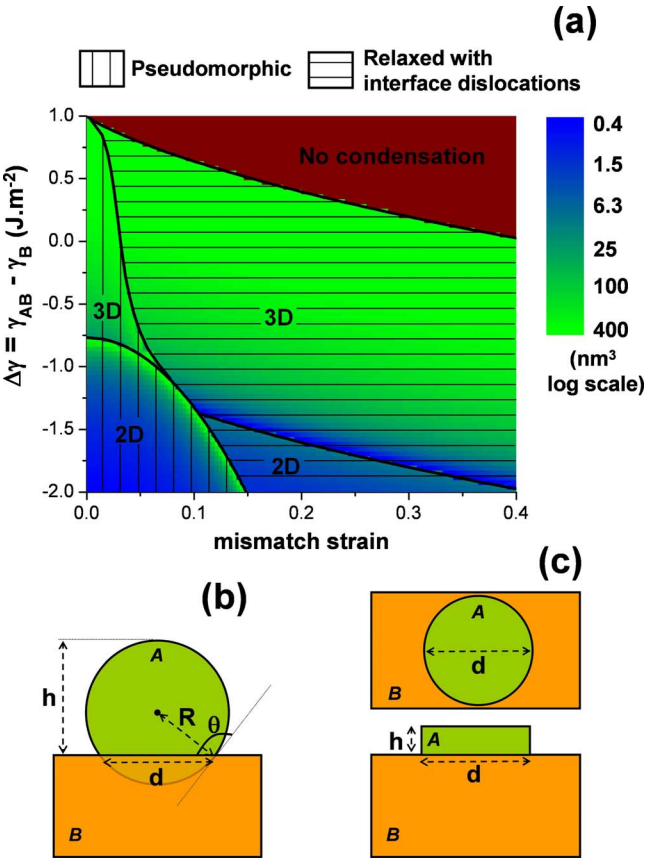

FIG. 1. (Color online) (a) Map of the critical volume (in nm^3, logarithmic scale), accommodation pathway and growth mode as a function of $\Delta\gamma=\gamma_{AB}-\gamma_B$ and mismatch strain, calculated using the Young moduli and Poisson ratios of InP for the deposit and STO for the substrate. (b) and (c) geometry of 3D and (2D) critical nuclei considered for the calculation.

$$V_C^{2D}=\frac{\pi}{4}\times a\times\left(\frac{2\cdot L}{1-\alpha_c-L/a\cdot(1+\alpha_B)}\right)^2, \tag{3}$$

where a is the monolayer height of the deposit, $\alpha_c=E_V/\Delta\mu$, $\alpha_B=(\gamma_{AB}-\gamma_B)/\gamma_i$, and $L=\gamma_i/\Delta\mu$. If the island is elastically strained on the substrate, E_V can be written as

$$E_V=\frac{Y_A}{1-\nu_A}\times e^2\times R=e\times \mathrm{m}^2\times R. \tag{4}$$

Where Y_A and υ_A are the Young modulus and Poisson ratio of the deposit, respectively, e is the lattice mismatch strain $[e=(a_{\mathrm{deposit}}-a_{\mathrm{substrate}})/a_{\mathrm{deposit}}]$ and R describes elastic energy relaxation at the free surfaces of the island. R can be expressed as $R=1-e^{-2kq}$, where $k=0.082$ for spherical caps, and $k=0.072$ for cylindrical islands.[28] In the case where the lattice mismatch is accommodated by an array of interfacial dislocations, $\alpha_c=0$, and α_B must be replaced by $\alpha_B^*=\alpha_B+\alpha_{\mathrm{dis}}$, where $\alpha_{\mathrm{dis}}=\frac{1}{\gamma_i}\times[e.b\cdot\frac{Y_A\cdot Y_B}{Y_A\cdot(1+\nu_B)+Y_B\cdot(1+\nu_A)}\cdot(\frac{1}{4\pi}\ln\frac{R_c}{b}+0.1)]$ accounts for the cost of formation of the dislocations, by units of surface. Y_B and ν_B are the Young modulus and Poisson ratio of the substrate and b is the Burger vector of the dislocations. For Lomer-Cottrell dislocations, $R_c=2b/e$ if the distance between two subsequent dislocations is smaller than the island height.

During the early stages of the growth, adatoms migrate on the surface and agglomerate. They form clusters that remain unstable (they dissociate very quickly) until the smallest critical nucleation size is reached. Thus, the growth mode (2D or 3D) and the accommodation pathway (elastic deformation or interface dislocations) are the ones that allow minimizing the critical nucleation volume. The map plotted in Fig. 1 illustrates the influence of the lattice mismatch and of the difference $\Delta\gamma=\gamma_{AB}-\gamma_B$ on the growth mode and accommodation pathway. It has been calculated using the Young moduli and Poisson ratios of $SrTiO_3$ for the substrate ($Y_B=238$ GPa, $\nu_B=0.23$),[29] of InP for the deposited material ($Y_A=61$ GPa, $\nu_A=0.36$),[30] a typical deposit surface energy of 1 $J.m^{-2}$ and a chemical potential difference $\Delta\mu=200$ meV per III-V atom pair. For each value of $\Delta\gamma$ and e, four critical nucleation volumes corresponding to the four possible configurations (2D or 3D, pseudomorphic growth or interface dislocations) were compared, and the configuration corresponding to the smallest critical nucleation volume was selected. Three-dimensional critical volumes were calculated by minimizing numerically expression (2) as a function of q.

The model proposed above is intended to demonstrate general trends in heteroepitaxial growth. For this reason, it is based on several simplifying hypotheses:

The shape of the nuclei is chosen for simplicity (spherical caps for three-dimensional nuclei, and cylinders for two-dimensional clusters). For a real system, the shape of the nuclei may depend on different parameters, particularly if the nuclei are facetted. Taking into account such effects is possible (using the Wulf construction),[31] but requires knowing the surface energies of all the possibly formed facets, which is not the case even for very well known materials. Moreover, such a treatment would considerably complicate the computation without bringing any significant additional comprehension.

For similar reasons, the surface energy of the nuclei is considered as uniform in our treatment. The surface energy has to be considered as the average value of the surface energies of all possibly formed facets.

Interface dislocations are quite simply described as perfect Lomer-Cottrell dislocations. The expression used to estimate their cost of formation is only valid if the distance between two subsequent dislocations is smaller than the height of the nuclei. This is supposed to be verified for quite large mismatches (that lead to the formation of dense arrays of interface dislocations) and for quite elevated interface energies (that lead to elevated critical nucleus volumes). Moreover, for very high mismatches (approaching 0.4), the notion of discrete dislocation becomes arguable. However, such elevated mismatches generally lead to the observation of epitaxial relationships that considerably decrease the effective lattice mismatch (this is in particular the case for the InP/STO system discussed in the following).

In the end, for the sake of simplification of the treatment, the step energies for the two-dimensional nuclei are described as the product of the area of their lateral face by a surface-energy term. In order not to loose in generality, and on the basis of arguments already discussed above, we have

chosen this surface energy equal to that of the top face of the cylinders.

Figure 1 shows that elevated mismatches and elevated interface energies (or low substrate surface energies) enhance accommodation by interface dislocations. Thus, as compared to the elastic deformation of the deposit, forming an interfacial array of dislocations allows localizing the deformation field on a much smaller region close to the interface, at the expense of the formation of interface dangling bonds. Thus, large lattice mismatches (which increase the cost of the elastic deformation) and large interface energies (which reduce the cost of breaking interfacial bonds) enhance the formation of interfacial dislocations. From the point of view of epitaxy, the possibility of accommodating the lattice mismatch by forming interface dislocations as soon as critical nuclei are formed opens important perspectives: the mismatched material takes its bulk parameter as soon as the growth begins, and does not undergo any plastic relaxation mechanism. Thus, contrasting with systems for which the lattice mismatch is accommodated by elastic deformation, threading defect free epitaxial growth can be obtained. However, for such systems, interface binding is expected to be weaker than for homogeneous systems. As a consequence, three-dimensional Vollmer-Weber like growth is enhanced [even if according to Fig. 1(a), a fully relaxed two-dimensional growth can also be achieved]. In the cases where the growth is initially three-dimensional, two-dimensional layers can be obtained by a controlled coalescence of the initially formed islands, but this coalescence process is liable to lead to the formation of threading defects. This will be discussed in further details in the next section and in the conclusion. Moreover, due to the elevated interface energy characteristic of highly dissimilar epitaxial systems, the most stable interface configuration is in competition with less stable, but possibly accessible, parasitic orientations. This is liable to produce multidomain growth, and in extreme cases, polycrystalline deposition.

III. EXPERIMENTAL STUDY OF THE InP/$SrTiO_3$ SYSTEM

We have studied the growth of InP on $SrTiO_3$(001) (STO) substrates. STO is a perovskite oxide (lattice parameter of 3.905 Å). The lattice mismatch between InP and STO exceeds 50% (the mismatch strain equals 33.4%) for a direct cube-on-cube heteroepitaxy. The growth, carried out by solid source molecular beam epitaxy (MBE) was monitored by reflection high-energy electron diffraction (RHEED). Before InP growth, the (001)-oriented STO substrates were etched in a buffered HF/NH_4F solution and carefully rinsed in deionized water. The substrates were then introduced in the MBE chamber and annealed under ultrahigh vacuum at 800 °C during 30 min. This treatment leads to the formation of an atomically flat TiO_2 terminated and $(2\times1)+(1\times2)$ reconstructed STO surface, as shown in Fig. 2. Elevated phosphorus partial pressures (typically of 10^{-5} Torr) and elevated growth rates (typically 1 μm.h^{-1}) are required at the beginning of the growth to ensure InP nucleation on the STO surface: for low growth rates and low phosphorus partial

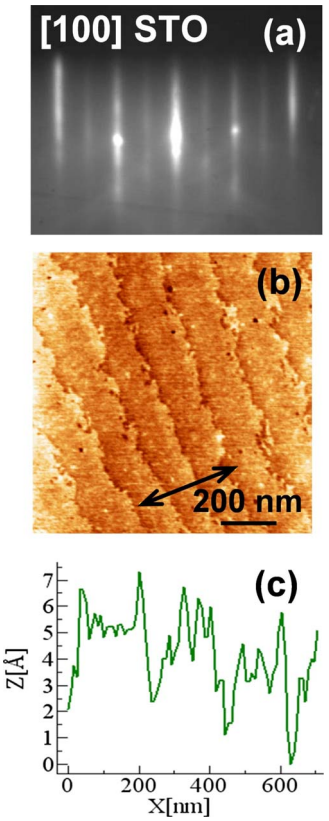

FIG. 2. (Color online) (a): RHEED pattern recorded along the [100] azimuth of the STO surface after thermal treatment at 800 °C during 30 min. The STO surface presents a clean $(2\times1)+(1\times2)$ surface reconstruction. (b) AFM image of the STO surface after annealing. The STO surface presents well defined atomic steps. A cross section of the image is displayed in (c) the average step height equals ≈4 Å, very close to the STO lattice parameter (3.905 Å).

pressures, RHEED systematically indicates delays in the InP nucleation (InP diffraction is observed a few seconds or even a few minutes after InP growth start). This is related to the large mismatch and large interface energy of the InP/STO system that leads to elevated critical nucleation volumes (Fig. 1): elevated $\Delta\mu$ (i.e., elevated growth rates and phosphorus partial pressures) are required to obtain significant nucleation rates due to the elevated critical nucleation volumes. Figure 3 shows the RHEED patterns observed after deposition of 3 monolayers of InP (growth rate of 1 μm.h^{-1}, phosphorus partial pressure of 10^{-5} Torr) at four different temperatures. All patterns are spotty as soon as the growth begins, indicating a three-dimensional growth in the Vollmer-Weber mode. At 350 and 390 °C, InP is principally (111) oriented on the (001)-oriented STO substrate. The presence of diffraction rings (particularly at 350 °C, but also at 390 °C) indicates the presence of random parasitic orientations in addition to the principal (111) InP orientation. At 430 and 480 °C, the RHEED patterns drastically change and correspond to well-ordered (001)-oriented InP. At 480 °C, an additional set of diffraction spots appears that corresponds to the presence of twins in InP.[32] It has to be noted that when deposited on an unreconstructed STO surface, InP is (111)-oriented for all deposition temperature.[20] (001)-oriented InP

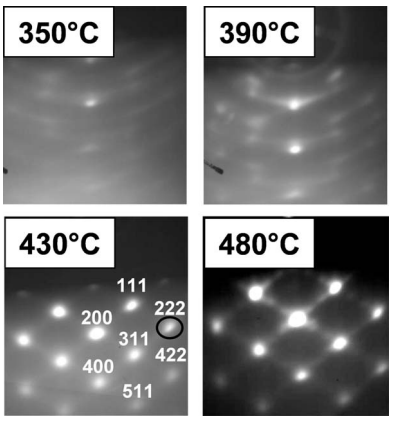

FIG. 3. RHEED patterns recorded after deposition of three monolayers of InP on STO under various temperatures. The InP 222 reflection (circled in the pattern recorded at 430 °C) was used to measure the evolution of the 222 interatomic distance at the early stages of InP growth [Fig. 4(a)].

can only be obtained on $(2\times1)+(1\times2)$-reconstructed STO surfaces, as detailed in Ref. 33. This brief analysis highlights the dependence of InP crystal orientation with the growth conditions, as expected for systems having large mismatches and large interface energies. It also shows that well oriented InP islands can be obtained on STO on condition that the growth conditions are perfectly controlled. Figure 4(a) shows the evolution of the InP d_{222} interatomic distance during InP deposition at 430 °C, as deduced from RHEED. According to this measurement, InP takes its bulk lattice parameter as soon as RHEED diffraction can be detected, after deposition of half a monolayer in the present case. High-resolution transmission electron microscopy (TEM) was used to characterize the InP/STO interface. The image displayed in Fig. 4(b) was recorded on a sample containing a 200 nm thick InP layer grown using the two-step method described in the following (first 4 nm of InP deposited at 430 °C at a growth rate of 1 μm.h^{-1}, and rest of the layer deposited at 480 °C). The interface is abrupt, and TEM electron diffraction pattern (not shown here) confirms that InP is (001)-oriented and presents its bulk lattice parameter. Moreover, InP aligns its [110] in-plane directions with the [100] in-plane directions of the STO substrate. At the growth temperature of the first 4 nm of InP and taking into account the thermal expansion coefficients for InP (Ref. 34) and STO,[35] a direct cube-on-cube epitaxial relationship between InP and STO would lead to a lattice mismatch of 50.02%. Most of this mismatch is accommodated by forming the abovementioned epitaxial relationship (which corresponds to a 45° in-plane rotation of the InP lattice with respect to the substrate). The residual mismatch (at 430 °C) equals 6.09%. A filtered Fourier-transform image of the interface is presented in the inset of Fig. 4(c). This image has been built by selecting the 200 STO and the 220 InP in plane reflections, so that only the lattice planes perpendicular to the interface are imaged. Regularly spaced localized lattice discontinuities can clearly be seen at the interface. These discontinuities correspond to the projections of the edge component of the Burger vector of geometric interface dislocations along the ⟨200⟩ STO in-plane direction. In

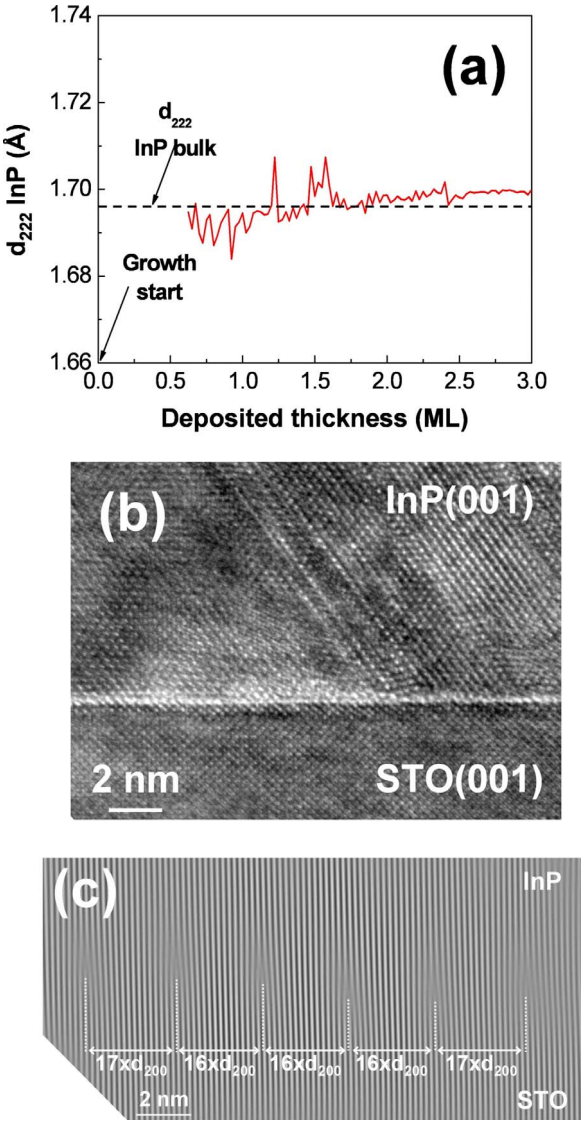

FIG. 4. (Color online) (a) Evolution of the 222 interatomic distance during the early stages of InP growth on STO (as deduced from RHEED). (b) High-resolution TEM cross-sectional view of an InP layer grown on STO. (c) Filtered Fourier-transform image of the heterointerface, obtained by selecting the STO 200 and InP 220 reflections (planes perpendicular to the interface).

average, one discontinuity is detected every 16.4 {200} STO planes (alternation of 16 and 17 {220} STO plane spacing between two subsequent discontinuities). The lattice mismatch accommodated by these geometric interface dislocations equals 6.09% and equals the effective lattice mismatch between InP and STO. As a consequence, the onset of the abovementioned epitaxial relationship, combined with the formation of an array of geometric interface dislocations accommodates the entire lattice mismatch between InP and STO. It has to be noted that similar effects have already been described for gold grain boundaries.[36] This accommodation pathway strongly contrasts with the one observed for standard III-V or IV-IV semiconductors, for which an initial elastic deformation of the lattice occurs, followed by a plastic relaxation process leading to the formation of large densities

of threading dislocations. Such a plastic relaxation mechanism does not occur during the growth of InP on STO, due to the fact that InP takes its bulk lattice parameter as soon as growth begins.

These experimental observations correspond to the theoretical prediction presented in Sec. II: the InP/STO system presents an elevated mismatch of more than 6% (considering the 45° rotated epitaxial relationship) and a large chemical heterogeneity (mostly related to the difference in crystal structure between both materials). For such systems, our model predicts a Vollmer-Weber three-dimensional nucleation and a misfit accommodation by interface dislocations, formed as soon as the material nucleates on the substrate. This matches our experimental observations. Such an accommodation pathway presents interesting features. In particular, there is no direct relationship between mismatch and density of threading defects, due to the fact that the growing material takes its bulk lattice parameter as soon as growth begins and does not undergo any plastic relaxation process. However, InP contains a large density of microtwins. A detailed discussion on the origin of these microtwins is beyond the topic of the present study and has been proposed elsewhere.[37] InP growth is initially three-dimensional and two-dimensional layers are formed by island coalescence. If the free surfaces of these islands present facets containing {111} planes, microtwin formation is enhanced during the coalescence step. These twins recombine quickly with each other at the early stages of the growth, so that their density decreases increasing the deposited thickness. The microtwin density equals a few 10^{11} cm^{-2} at the InP/STO interface, and decreases down to a few 10^{7} cm^{-2} for an InP thickness of 1 μm.

An InAsP/InP quantum well structure was grown on a STO(001) substrate in a two step growth. The first 4 nm of InP were deposited at 430 °C at a growth rate of 1 $\mu m.h^{-1}$ and under a phosphorus partial pressure of 10^{-5} Torr. This leads to the formation of (001)-oriented InP islands and allows minimizing the twin density, according to the RHEED images displayed in Fig. 3. 1 μm of InP were then deposited at 480 °C. At the beginning of this second growth step, the InP islands formed during the first step coalesce to form a two-dimensional thin film. In the well referenced case where quantum dots are formed in the Stranski-Krastanov growth mode, such coalescence is well known as leading to the formation of defects in the coalesced layer. The origin of these defects is related to the fact that the coalescing islands are still partly strained when then coalesce. The differences in the relaxation rate of two neighboring islands, combined with the residual strain in the material, lead to the formation of defects and to a strong roughening of the growth front. In contrast here, the coalescing islands have their bulk lattice parameter and are not deformed. As a consequence, two coalescing islands have the same in- and out-of-plane lattice parameters. However, even if none of our structural analyses of the coalesced InP layers has revealed defects specifically related to this coalescence process, one can expect that threading defects are formed during coalescence: there is *a priori* no lateral registry between the interface dislocation arrays of two coalescing islands. As a consequence, when coalescence occurs, interface dislocations must glide in the interface plane to join one with another and form a continuous network. This is only possible if the interface plane is an easy gliding plane, which is *a priori* not the case. Thus, additional threading dislocation segments are probably formed during coalescence, due to the lack of translational registry between the interface dislocation networks of two neighboring islands. Solutions are proposed in the conclusion to circumvent this difficulty.

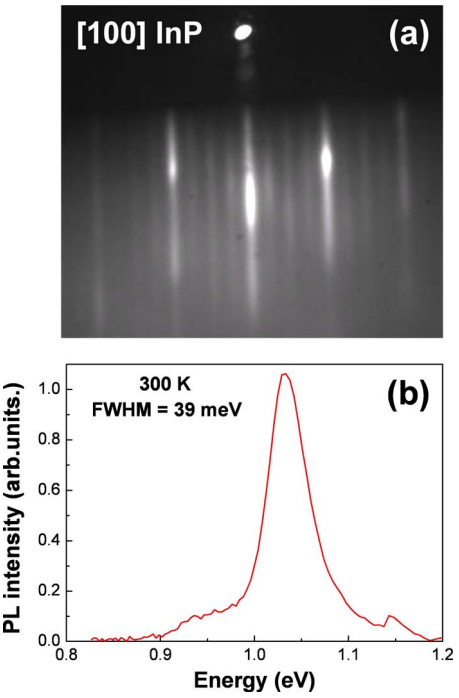

FIG. 5. (Color online) (a) RHEED pattern recorded on InP [100] azimuth after the deposition of 500 nm of InP. (b) Room-temperature photoluminescence spectrum of an InAsP/InP quantum well grown on STO(001).

An InAsP quantum well was grown on the 1 μm thick coalesced InP layer, and embedded in a 50-nm-thick InP layer. The RHEED pattern presented in Fig. 5(a) was recorded after deposition of 500 nm on InP at 480 °C. It presents streaky lines and a bright times four reconstruction, indicating a complete coalescence of the initially formed islands and the recovery of a perfectly flat growth front. The room-temperature photoluminescence spectrum of the quantum well is presented in Fig. 5(b). Its full width at half maximum is 39 meV; equivalent to that of an equivalent quantum well grown on a native InP substrate. This result attests of the good optical quality of the heterostructure.

IV. CONCLUSION

It appears to be profitable to take advantage of the large lattice mismatch and the chemical heterogeneity between two crystalline materials to enhance the formation of interface dislocations at the very early stages of the growth, when the material nucleates. In this configuration, the growing material takes its bulk lattice parameter as soon as growth begins and does not undergo any plastic relaxation mechanism that degrades its structural and electronic properties. Our experimental results concerning the InP/STO system open the

way to the monolithic integration of InP on silicon using STO/Si crystalline buffers. They show that the spontaneous tendency of this "weakly bound" system to enhance crystalline disorder can be managed, that a controlled coalescence of the initially formed three-dimensional islands can be achieved, and that good optical quality can be obtained despite the very large lattice mismatch. Some of our preliminary studies indicate that the GaAs/STO system exhibit similar behavior, showing that lattice mismatch has no direct influence on the growth and structural properties of highly dissimilar epitaxial systems. The issue of the formation of defects during the coalescence step due to the lack in lateral registry between the dislocation networks of two neighboring islands has to be addressed. A first solution consists in reducing the density of such defects by reducing the density of islands formed before the coalescence step. Such a solution could be compatible with the fabrication of micron-sized optoelectronic devices such as microdisk based lasers. Another solution consists in enhancing a two-dimensional step-flow growth of the semiconductor on the oxide template. In such a case, the interface dislocation array will be progressively formed during the formation of the first InP monolayer[38] and the oxide surface will be entirely covered without any coalescence process. A two-dimensional growth mode can be promoted by increasing the wetting during the initial stages of the growth (use of surfactants, increase in the substrate surface energy by treating the substrate surface before growth…). Even if the growth is initially three dimensional, the formation of coalescence defects can be avoided by obtaining the coalescence at the very early stages of the growth, when the initially formed 3D islands are very small: if the average lateral size of the islands is smaller than the average distance between two subsequent dislocations (approximately 3.5 nm in the InP/STO case) when coalescence occurs, the array of interface dislocations will be formed once the STO surface is entirely covered by InP. This should allow circumventing the problem of the formation of defects during the coalescence. To obtain such a situation, the density of initially formed InP islands must be increased by reducing the adatom diffusion length (increase in the growth rate and phosphorus partial pressure, for example), and by enhancing the wetting.

ACKNOWLEDGMENTS

The authors gratefully thank Michel Gendry for useful discussions, as well as Claude Botella and Jean-Baptiste Goure for technical assistance. This work was supported by the Nanolyon technology platform, and partly financed by the French "Agence Nationale de la Recherche" (project "BOTOX" #JCJC-0055).

*Corresponding author; guillaume.saint-girons@ec-lyon.fr

[1] J. Narayan and B. C. Larson, J. Appl. Phys. **93**, 278 (2003).
[2] J. W. Matthews and A. E. Blakeslee, J. Cryst. Growth **27**, 118 (1974).
[3] D. G. Deppe, N. Holonyak, D. W. Nam, K. C. Hsieh *et al.*, Appl. Phys. Lett. **51**, 637 (1987).
[4] S. M. Ting and E. A. Fitzgerald, J. Appl. Phys. **87**, 2618 (2000).
[5] M. E. Groenert, C. W. Leitz, A. J. Pitura, V. Yang *et al.*, J. Appl. Phys. **93**, 362 (2003).
[6] Y. H. Lo, Appl. Phys. Lett. **59**, 2311 (1991).
[7] S. Rohart, G. Grenet, and C. Priester, Appl. Surf. Sci. **188**, 193 (2002).
[8] M. Kostrzewa, G. Grenet, P. Regreny, J. L. Leclercq *et al.*, J. Cryst. Growth **275**, 157 (2005).
[9] J. Bai, J.-S. Park, Z. Cheng, M. Curtin *et al.*, Appl. Phys. Lett. **90**, 101902 (2007).
[10] A. Trampert, Physica E **13**, 1119 (2002).
[11] A. Trampert and K. H. Ploog, Cryst. Res. Technol. **35**, 793 (2000).
[12] C. Palmstrom, Annu. Rev. Mater. Sci. **25**, 389 (1995).
[13] S.-W. Chan, J. Phys. Chem. Solids **55**, 1137 (1994).
[14] R. A. McKee, F. J. Walker, and M. F. Chisholm, Phys. Rev. Lett. **81**, 3014 (1998).
[15] G. Delhaye, C. Merckling, M. El-Kazzi, G. Saint-Girons *et al.*, J. Appl. Phys. **100**, 124109 (2006).
[16] G. J. Norga, C. Marchiori, C. Rossel, A. Guiller *et al.*, J. Appl. Phys. **99**, 084102 (2006).
[17] K. Eisenbeiser, R. Emrick, R. Droopad, Z. Yu *et al.*, IEEE Electron Device Lett. **23**, 300 (2002).
[18] D. C. Jordan, R. Droopad, Z. Yu, and C. Overgaard, US Patent No. US2002/0163024A1.
[19] Z. Yu, R. Droopad, and W. J. Ooms, US Patent No. US2002/0153524A1.
[20] G. Saint-Girons, C. Priester, P. Regreny, G. Patriarche *et al.*, Appl. Phys. Lett. **92**, 241907 (2008).
[21] G. Saint-Girons, P. Regreny, L. Largeau, G. Patriarche *et al.*, Appl. Phys. Lett. **91**, 241912 (2007).
[22] M. H. Grabow and G. H. Gilmer, Surf. Sci. **194**, 333 (1988).
[23] K. Nakajima, Jpn. J. Appl. Phys. **38**, 1875 (1999).
[24] V. A. Shchukin, N. N. Ledentsov, P. S. Kop'ev, and D. Bimberg, Phys. Rev. Lett. **75**, 2968 (1995).
[25] H. Mariette, C. R. Phys. **6**, 23 (2005).
[26] I. Daruka and A. L. Barabási, Phys. Rev. Lett. **79**, 3708 (1997).
[27] G. Wulf, Z. Kristallogr. **34**, 449 (1901).
[28] K. Tillmann and A. Förster, Thin Solid Films **368**, 93 (2000).
[29] S. R. Jian, W. J. Chang, T. H. Fang, L. W. Ji *et al.*, Mater. Sci. Eng., B **131**, 281 (2006).
[30] D. N. Nichols, D. S. Rimai, and R. J. Sladek, Solid State Commun. **36**, 667 (1980).
[31] P. Müller and R. Kern, Appl. Surf. Sci. **162-163**, 133 (2000).
[32] The origin of these twins will be discussed in a forthcoming paper.
[33] J. Cheng, P. Regreny, L. Largeau, G. Patriarche, O. Mauguin, K. Naji, G. Hollinger, and G. Saint-Girons, J. Cryst. Growth **311**, 1042 (2009).
[34] V. M. Glazov, K. Davletov, A. Y. Nashelskii, and M. M. Mamedov, Zh. Fiz. Khim. **51**, 2558 (1977).
[35] K. Munakata and A. Okazaki, Acta Crystallogr., Sect. A: Found. Crystallogr. **A60**, 33 (2004).
[36] L. Priester, Rev. Phys. Appl. **15**, 789 (1980).
[37] J. Cheng, L. Largeau, G. Patriarche, P. Regreny, G. Hollinger, and G. Saint-Girons, Appl. Phys. Lett. **94**, 231902 (2009).
[38] F. K. LeGoues *et al.*, Appl. Phys. Lett. **67**, 2317 (1995).